Title page:

NeuroMark: an adaptive independent component analysis framework for estimating reproducible and comparable fMRI biomarkers among brain disorders

Yuhui Du[1,2*,#], Zening Fu[2,#], Jing Sui[2,3], Shuang Gao[3], Ying Xing[1], Dongdong Lin[2], Mustafa Salman[2,4], Md Abdur Rahaman[2], Anees Abrol[2], Jiayu Chen[2], L Elliot Hong[5], Peter Kochunov[5], Elizabeth A. Osuch[6], Vince D. Calhoun[2], for the Alzheimer's Disease Neuroimaging Initiative※

[1]*School of Computer and Information Technology, Shanxi University, Taiyuan, China*

[2]*Tri-Institutional Center for Translational Research in Neuroimaging and Data Science (TReNDS),Georgia State University, Georgia Institute of Technology, Emory University, Atlanta, GA, USA*

[3]*Chinese Academy of Sciences (CAS) Centre for Excellence in Brain Science and Intelligence Technology; University of Chinese Academy of Sciences; Institute of Automation, CAS; China*

[4]*School of Electrical & Computer Engineering, Georgia Institute of Technology, Atlanta, USA*

[5]*University of Maryland Center for Brain Imaging Research, Baltimore, USA*

[6]*Lawson Health Research Institute, London Health Sciences Centre, London, Canada*

*** *Corresponding author：***

Yuhui Du, School of Computer and Information Technology, Shanxi University, Taiyuan, China, duyuhui@sxu.edu.cn

 # *Co-first authors:*

Yuhui Du and Zening Fu

※Data in Study 3 used in preparation of this article were obtained from the Alzheimer's Disease Neuroimaging Initiative (ADNI) database (adni.loni.usc.edu). As such, the investigators within the ADNI contributed to the design and implementation of ADNI and/or provided data but did not participate in analysis or writing of this report. A complete listing of ADNI investigators can be found at:

http://adni.loni.usc.edu/wp-content/uploads/how_to_apply/ADNI_Acknowledgement_List.pdf

NeuroMark: an adaptive independent component analysis framework for estimating reproducible and comparable fMRI biomarkers among brain disorders

Yuhui Du[1,2*,#], Zening Fu[2,#], Jing Sui[2,3], Shuang Gao[3], Ying Xing[1], Dongdong Lin[2], Mustafa Salman[2,4], Md Abdur Rahaman[2], Anees Abrol[2], Jiayu Chen[2], L Elliot Hong[5], Peter Kochunov[5], Elizabeth A. Osuch[6], Vince D. Calhoun[2], for the Alzheimer's Disease Neuroimaging Initiative※

[1]*School of Computer and Information Technology, Shanxi University, Taiyuan, China*

[2]*Tri-Institutional Center for Translational Research in Neuroimaging and Data Science (TReNDS),Georgia State University, Georgia Institute of Technology, Emory University, Atlanta, GA, USA*

[3]*Chinese Academy of Sciences (CAS) Centre for Excellence in Brain Science and Intelligence Technology; University of Chinese Academy of Sciences; Institute of Automation, CAS; China*

[4]*School of Electrical & Computer Engineering, Georgia Institute of Technology, Atlanta, USA*

[5]*University of Maryland Center for Brain Imaging Research, Baltimore, USA*

[6]*Lawson Health Research Institute, London Health Sciences Centre, London, Canada*

Abstract

Increasing data-sharing initiatives have provided unprecedented opportunities to study brain disorders. Standardized approaches for capturing reproducible and comparable biomarkers are greatly needed in big-data analysis. Here, we propose a framework (called *NeuroMark*) that leverages a priori-driven independent component analysis (ICA) to extract functional brain network features from fMRI data. *NeuroMark* estimates features adaptable to each individual and comparable across subjects by taking advantage of the replicated brain network templates extracted from 1828 healthy controls. Four studies including 2454 subjects were conducted, spanning six brain disorders (schizophrenia, autism spectrum disorder, depression, bipolar disorder, mild cognitive impairment and Alzheimer's disease) to evaluate the proposed framework from different perspectives (replication, cross-study comparison, subtle difference identification, and multi-disorder classification). Our results demonstrate the great potential of *NeuroMark* to identify reproducible and comparable brain network markers, its feasibility to link results across different datasets/studies/disorders, and its sensitivity in identifying biomarkers for patients with challenging mental illnesses.

Main

In the neuroscience field, increasing data-sharing initiatives have accelerated the use of neuroimaging to study brain disorders in the clinic [1-3]. Access to multi-site datasets affords unprecedented opportunities to perform large-scale analysis across disorders. However, systematic methods to estimate neuroimaging measures in the context of enhancing neuroscientific validity are still very limited. There is a need for techniques that can accelerate the identification of interpretable brain markers in preexisting data and evaluation for the generalizability, reproducibility and their relationship to other data.

Abundant approaches have been utilized to capture neuroimaging features informative of brain functional connectivity, including region of interest (ROI) or seed derived connectivity analysis [4, 5], self-activation detection method (such as amplitude of low frequency fluctuation and regional homogeneity [6]), decomposition-based independent component analysis (ICA) [7-9], as well as clustering techniques to group brain voxels[10]. Particularly, ROI analysis and ICA are the most common approaches to explore functional organization of brain. While ROI-based methods typically require fixed brain regions according to prior experience or knowledge, ICA, a data-driven method, is capable of capturing functional networks while retaining more single-subject variability [11]. ICA leverages the hidden spatio-temporal information to extract maximally spatially independent components (ICs), each of which includes brain voxels sharing co-varying patterns. Other advantages of ICA are that it can achieve intrinsic connectivity network (ICN) extraction and noise component removal simultaneously [12], and enable separation of overlapping but distinct functional activity [13]. However, blind ICA is challenging for multi-subject analyses, since components extracted from different subjects may not have spatial correspondence. To overcome the ICA correspondence limitation, we and others have developed group ICA methods [9, 14-16]. The majority of these approaches involve an ICA performed on the group data to estimate the group-level components, and then utilize a back-reconstruction method to extract individual-level functional networks and corresponding time-courses.

Group ICA still has limitations since comparing results from different group ICA is not straightforward, affecting the abilities to replicate findings from different studies. For example, a study [17] identified 50 ICNs arranged into seven functional domains, and another study [18]

characterized 52 ICNs sorted to three domains, despite using the same model order. Such differences in the identified ICNs and their arrangements hinder the direct comparisons across the results. The non-correspondence between group ICA runs also leads to a problem in studies focusing on classification where group ICA was usually performed on all subjects to make the resulting features work for the trained classifier [19, 20]. This operation can be biased as the feature extraction should be independent from the testing data.

From a clinical perspective, although some brain disorders can be assigned to distinct categories, many share clinically-overlapping symptoms. It is beneficial to investigate the shared/unique brain alterations among them and develop biologically-based subtypes across psychotic illnesses [21]. For example, both schizoaffective and bipolar disorders experience hallucinations and delusions that are typical features of schizophrenia (SZ) [22], which can make their clinical differentiation difficult. SZ and autism spectrum disorder (ASD) currently conceptualized as distinct illnesses have also been revisited in recent years due to their shared phenotypic and genotypic expression [23]. There is a paucity of studies that perform a direct comparison of symptom-related disorders and the validation of brain changes, probably due to the limited ability of analytic methods to characterize individual variability [24] and reliability [25]. Since more neuroimaging data are now available than ever before, we have an opportunity to probe this aim. A framework that can optimize the data-specific variability while retaining the comparability across different datasets, studies and disorders is needed.

In this paper, we propose *NeuroMark,* a framework that can leverage group information guided ICA (GIG-ICA) [16] or spatially constrained ICA [26] based on spatial priors derived from independent large samples to adaptively estimate individual network features (called Adaptive-ICA). We conducted four studies to validate the reliable performance of *NeuroMark* in different ways (replication, cross-study comparison, subtle difference extraction, and multi-disorder classification). Our results highlighted that *Neuromark* enables the replication of identified biomarkers across different datasets, the link from evaluating results on different studies, the identification of subtle brain functional impairments, and the effective differentiation between multiple disorders with confounding symptoms. *NeuroMark* can contribute to our understanding of the commonality, specificity, and inter-relationship among different brain disorders. While we focus on resting fMRI

initially, *NeuroMark* can be expanded to incorporate multimodal imaging data as well. The code and templates are available online (www.yuhuidu.com and http://trendscenter.org/software).

Results

The flowchart of the *NeuroMark* is displayed in Fig. 1. First, replicated ICN templates are constructed from different groups of large-sample healthy controls (HCs). Next, using the ICN templates as the spatial network priors, GIG-ICA [12, 16] is applied for Adaptive-ICA to estimate subject-specific functional networks and associated time-courses (TCs), due to high reliability [27] and accurate individual property [28] of the networks estimated by the method. Finally, different functional network features such as functional network connectivity (FNC) are computed and evaluated.

We obtained 53 replicated network templates (Fig. 2) that are common between 823 HCs in the human connectome project (HCP) and 1005 HCs in the genomics superstruct project (GSP) datasets. They were arranged into seven functional domains according to their functional and anatomical roles [17], including the sub-cortical (SC: 5 ICNs), auditory (AU: 2 ICNs), sensorimotor (SM: 9 ICNs), visual (VI: 9 ICNs), cognitive control (CC: 17 ICNs), default mode (DM: 7 ICNs) and cerebellar (CB: 4 ICNs) domains. The detailed component labels and peak coordinates are provided in Table 1. We evaluate the framework using four studies, showing that *NeuroMark* provides an effective approach to identify and compare brain biomarkers.

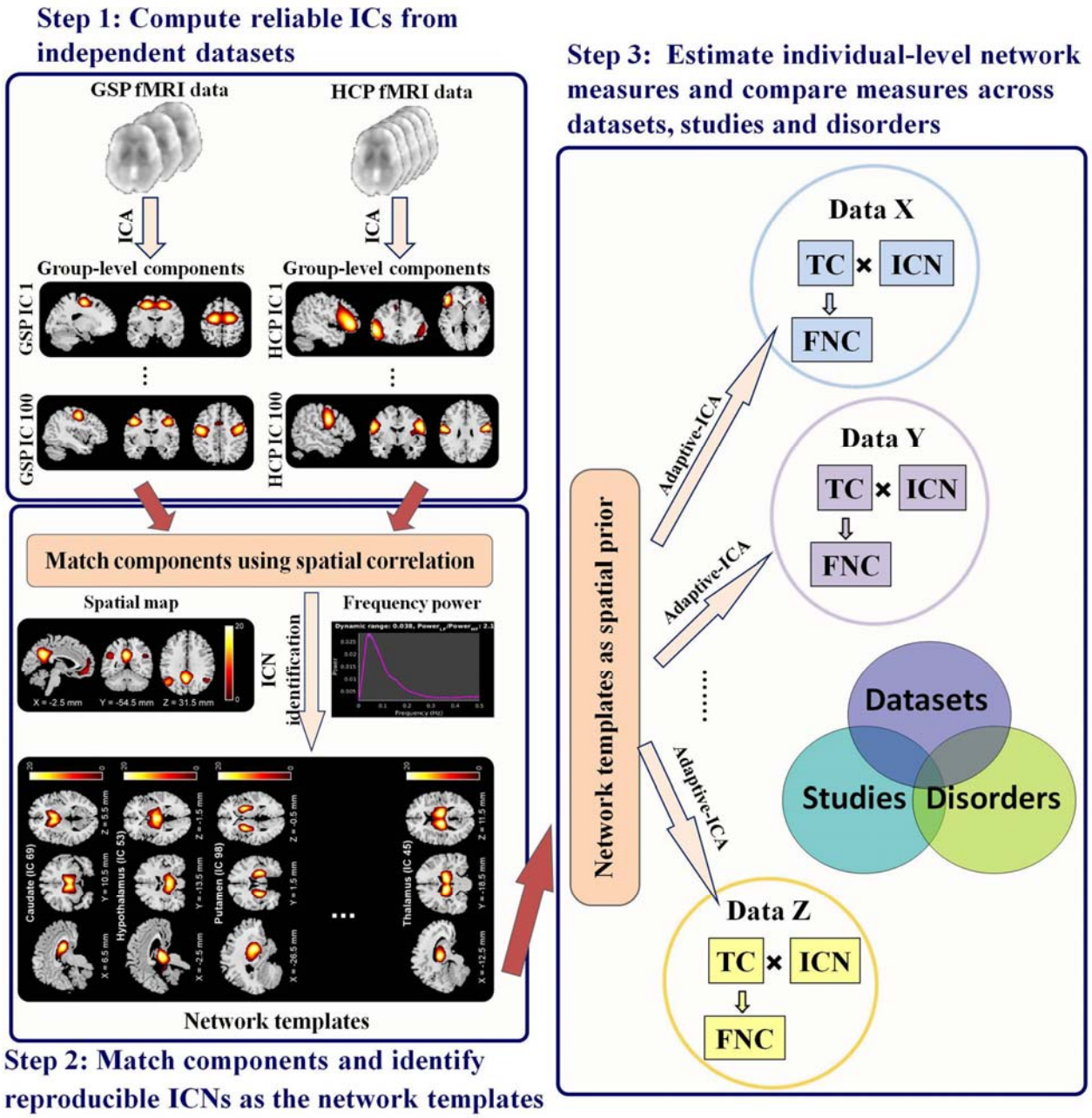

Fig. 1. Schematic flowchart of the proposed framework. Step 1: Calculate group-level independent components (ICs) from two independent datasets with large sample of healthy controls including the human connectome project (HCP) and genomics superstruct project (GSP) datasets; Step 2: Match ICs using spatial correlations between their spatial maps and identify highly replicated intrinsic connectivity networks (ICNs) as the network templates; Step 3: Calculate the individual-level ICNs and their related time courses (TCs) by taking the network templates as prior information in Adaptive-ICA. Other extended features such as functional network connectivity (FNC) can be obtained and then compared across datasets, studies, and disorders.

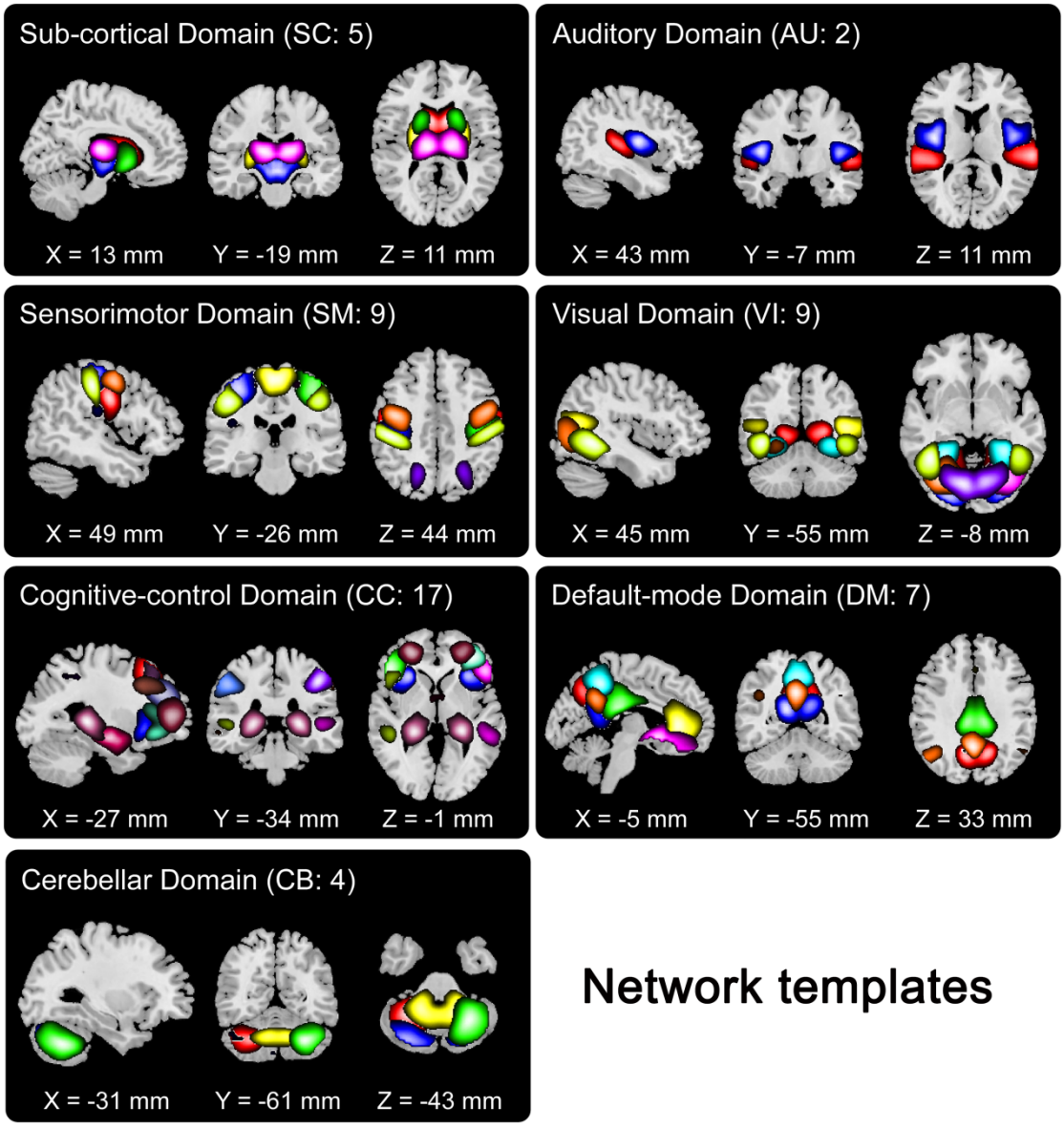

Fig. 2. Visualization of the identified network templates, which were divided into seven functional domains based on their anatomical and functional properties. In each subfigure, one color in the composite maps corresponds to an ICN.

Table 1. Information of the extracted network templates. For each template, its functional domain, primary brain region and peak coordinate are included. Here, each network template is represented by one independent component (IC). IC ID is shown along with the brain region name.

Primary regions in ICNs (IC ID)	X	Y	Z	Primary regions in ICNs (IC ID)	X	Y	Z
Sub-cortical domain (SC)				**Cognitive-control domain (CC)**			
Caudate (IC 69)	6.5	10.5	5.5	Inferior parietal lobule ([IPL], IC 68)	45.5	-61.5	43.5
Subthalamus/hypothalamus (IC 53)	-2.5	-13.5	-1.5	Insula (IC 33)	-30.5	22.5	-3.5

Putamen (IC 98)	-26.5	1.5	-0.5	Superior medial frontal gyrus ([SMFG], IC 43)	-0.5	50.5	29.5
Caudate (IC 99)	21.5	10.5	-3.5	Inferior frontal gyrus ([IFG], IC 70)	-48.5	34.5	-0.5
Thalamus (IC 45)	-12.5	-18.5	11.5	Right inferior frontal gyrus ([R IFG], IC 61)	53.5	22.5	13.5
Auditory domain (AU)				Middle frontal gyrus ([MiFG], IC 55)	-41.5	19.5	26.5
Superior temporal gyrus ([STG], IC 21)	62.5	-22.5	7.5	Inferior parietal lobule ([IPL], IC 63)	-53.5	-49.5	43.5
Middle temporal gyrus ([MTG], IC 56)	-42.5	-6.5	10.5	Left inferior parietal lobue ([R IPL], IC 79)	44.5	-34.5	46.5
Sensorimotor domain (SM)				Supplementary motor area ([SMA], IC 84)	-6.5	13.5	64.5
Postcentral gyrus ([PoCG], IC 3)	56.5	-4.5	28.5	Superior frontal gyrus ([SFG], IC 96)	-24.5	26.5	49.5
Left postcentral gyrus ([L PoCG], IC 9)	-38.5	-22.5	56.5	Middle frontal gyrus ([MiFG], IC 88)	30.5	41.5	28.5
Paracentral lobule ([ParaCL], IC 2)	0.5	-22.5	65.5	Hippocampus ([HiPP], IC 48)	23.5	-9.5	-16.5
Right postcentral gyrus ([R PoCG], IC 11)	38.5	-19.5	55.5	Left inferior parietal lobue ([L IPL], IC 81)	45.5	-61.5	43.5
Superior parietal lobule ([SPL], IC 27)	-18.5	-43.5	65.5	Middle cingulate cortex ([MCC], IC 37)	-15.5	20.5	37.5
Paracentral lobule ([ParaCL], IC 54)	-18.5	-9.5	56.5	Inferior frontal gyrus ([IFG], IC 67)	39.5	44.5	-0.5
Precentral gyrus ([PreCG], IC 66)	-42.5	-7.5	46.5	Middle frontal gyrus ([MiFG], IC 38)	-26.5	47.5	5.5
Superior parietal lobule ([SPL], IC 80)	20.5	-63.5	58.5	Hippocampus ([HiPP], IC 83)	-24.5	-36.5	1.5
Postcentral gyrus ([PoCG], IC 72)	-47.5	-27.5	43.5	**Default-mode domain (DM)**			
Visual domain (VI)				Precuneus (IC 32)	-8.5	-66.5	35.5
Calcarine gyrus ([CalcarineG], IC 16)	-12.5	-66.5	8.5	Precuneus (IC 40)	-12.5	-54.5	14.5
Middle occipital gyrus ([MOG], IC 5)	-23.5	-93.5	-0.5	Anterior cingulate cortex ([ACC], IC 23)	-2.5	35.5	2.5
Middle temporal gyrus ([MTG], IC 62)	48.5	-60.5	10.5	Posterior cingulate cortex ([PCC], IC 71)	-5.5	-28.5	26.5
Cuneus (IC 15)	15.5	-91.5	22.5	Anterior cingulate cortex ([ACC], IC 17)	-9.5	46.5	-10.5
Right middle occipital gyrus ([R MOG], IC 12)	38.5	-73.5	6.5	Precuneus (IC 51)	-0.5	-48.5	49.5
Fusiform gyrus (IC 93)	29.5	-42.5	-12.5	Posterior cingulate cortex ([PCC], IC 94)	-2.5	54.5	31.5
Inferior occipital gyrus ([IOG], IC 20)	-36.5	-76.5	-4.5	**Cerebellar domain (CB)**			
Lingual gyrus ([LingualG], IC 8)	-8.5	-81.5	-4.5	Cerebellum ([CB], IC 13)	-30.5	-54.5	-42.5
Middle temporal gyrus ([MTG], IC 77)	-44.5	-57.5	-7.5	Cerebellum ([CB], IC 18)	-32.5	-79.5	-37.5
				Cerebellum ([CB], IC 4)	20.5	-48.5	-40.5
				Cerebellum ([CB], IC 7)	30.5	-63.5	-40.5

Study 1: SZ patients show significant and replicable static FNC alterations using different datasets

In the study, we assess the ability of our framework to identify reproducible biomarkers using the Function Biomedical Informatics Research Network (FBIRN) dataset including 137 SZ patients and 144 HCs and another dataset collected at the University of Maryland, Maryland Psychiatric Research Center (MPRC) including 150 SZ patients and 238 HCs. Static FNC (sFNC), computed using the whole time series of all ICNs, was obtained to reflect the interaction between networks for each subject. The sFNC pattern showed consistency between FBIRN and MPRC, as shown in Fig. 3(A) and (D), indicating their comparability. For FBIRN, we compared the differences between HC

and SZ by performing two-sample t-tests on sFNC. Fig. 3(B) and (C) display the original HC vs. SZ T-value map for all sFNC and the significant differences after the multiple comparisons correction, respectively. Similar results were found from the MPRC as shown in Fig. 3(E) and (F), supporting that the results are reproducible although the FBIRN dataset showed more significant differences.

The primary brain functional impairments in SZ from both datasets were consistently located in the connectivity between the SC and CB domains, between the SC and AU domains, as well as between the SC and SM domains. We identified the common sFNC alterations of SZ for both the FBIRN and MPRC data by evaluating the results in Fig. 3(C) and (F). Our results (Fig. 3(G)) indicate that the sFNC mean value of SZ was close between FBRIN and MPRC, although FBIRN data slightly showed enhanced connection strengths than MPRC data. Compared to HC, SZ showed 1) decreased positive connectivity between the SC and CB domains, 2) diminished negative connectivity between the SC and AU domains, between the SC and SM domains, and 3) positive connection between the superior temporal gyrus and thalamus (in contrast to HC with negative connection). Taken together, our results suggest that the *NeuroMark* framework was able to identify reproducible network markers.

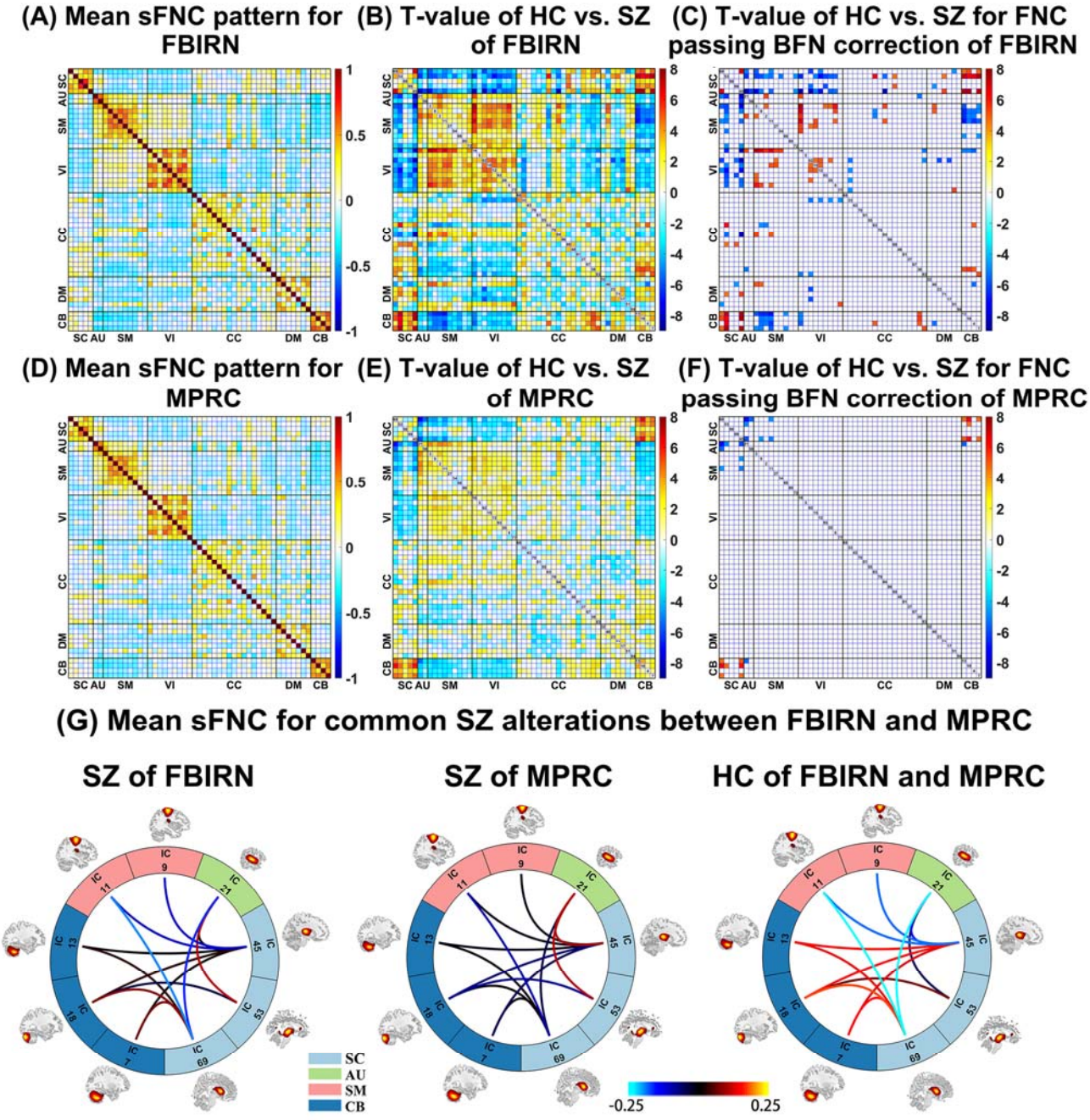

Fig. 3. Result of study 1, which shows that there are reproducible sFNC alterations of SZ between FBIRN and MPRC data. (A) and (D): Mean sFNC pattern across all subjects for FBIRN and MPRC, respectively. (B) and (E): The T-values of all sFNCs from two-sample t-tests for FBIRN and MPRC, respectively. (C) and (F): The T-values for the remaining FNCs after the multiple comparisons correction ($p < 0.05$ with Bonferroni correction) for FBIRN and MPRC, respectively. "BFN" denotes Bonferroni correction. (G): The mean sFNC in the common impairments of SZ between FBIRN and MPRC data. For each commonly impaired sFNC, the averaged value in SZ patients of FBIRN, SZ patients of MPRC, and HCs of the two datasets is shown, respectively.

Study 2: ASD and SZ show common sFNC impairments

In this study, we highlight the potential for using *NeuroMark* to link results across different studies. We evaluated sFNC changes in ASD using 398 ASD patients and 471 HCs from Autism Brain Imaging Data Exchange I (ABIDEI), and then compared the abnormalities between SZ and ASD by linking study 1 and 2. The mean sFNC of ABIDEI data (Fig. 4(A)) shows a similar connectivity pattern with that from study 1. By performing statistical analysis, significant changes in ASD relative to HC were found, primarily involving the SC, CB, AU and SM domains, as shown in Fig. 4(B) and (C).

While study 2 could stand on its own as a result, we were interested in learning additional information by linking study 1 and 2. By comparing the common HC vs. SZ connection differences in both FBIRN and MPRC with the HC vs. ASD connection differences from ABIDEI, we identified nine common sFNC alterations between SZ and ASD relative to HC. As illustrated in Fig. 4(D), for both SZ and ASD patients, the sub-cortical, sensorimotor, auditory and cerebellar regions related sFNC were commonly affected. The sub-cortical regions showed the largest number of common impairments across the two disorders.

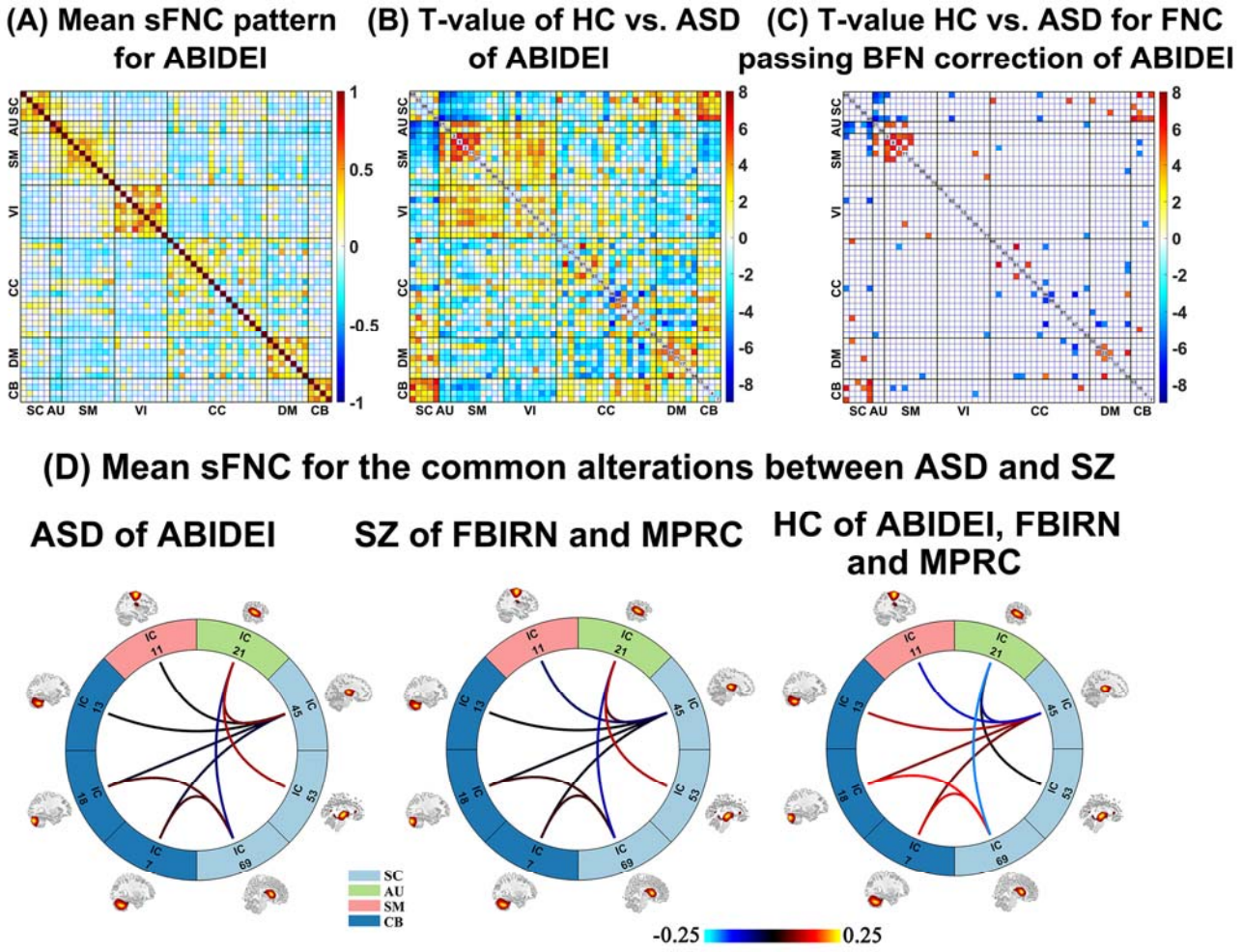

Fig. 4. Results of study 2, which supports that SZ and ASD show common alterations in sFNC. (A): Mean sFNC pattern across all subjects for ABIDEI. (B) and (C): The T-values of all sFNCs and that of the remaining sFNCs after the multiple comparisons correction ($p < 0.05$ with Bonferroni correction) from two-sample t-tests of HC vs. ASD for ABIDEI. "BFN" denotes Bonferroni correction. (D) Mean sFNC of each group (ASD, SZ and HC) in the overlapping impairments between SZ and ASD. For each commonly impaired sFNC, the averaged value in ASD patients of ABIDEI, SZ patients of FBIRN and MPRC, and HCs of the three datasets is shown, respectively.

Study 3: Mild cognitive impairment (MCI) demonstrates intermediate dynamic FNC changes between HC and Alzheimer's disease (AD)

In this study, we aim to show that our framework can effectively capture subtle differences in dynamic functional network connectivity (dFNC) among multiple groups. The analysis focused on Alzheimer's disease (AD) and mild cognitive impairment (MCI) using the Alzheimer's Disease Neuroimaging Initiative (ADNI) dataset.

Using 104 AD patients, 470 MCI patients, and 264 HCs, the dFNC patterns were computed using a sliding-window method based on the time-series of individual-subject networks extracted by

NeuroMark. Next, the reliable connectivity states were extracted from dFNC using a clustering technique. In the group-discriminating states (Fig. 5), specifically the state 2 that accounts for >50% of all windows resembled the sFNC patterns; the state 1 revealed negative connectivity between SM and VI; and the state 3 in contrast showed a strong connection between SM and VI. Compared to HCs, AD patients had a significantly different fraction rate of occurrences in dFNC states. In general, AD patients spent less time in strongly-connected states (i.e. state 1 and state 3 showing strong correlated and anticorrelated connectivity patterns) but more time in weakly-connected states (state 2 and state 5). Although there was no significant group difference in the occurrences between MCI and HC/AD, MCI showed a similar but weaker trend with AD. Looking into it further, when separating MCI groups into early MCI (EMCI) and late MCI (LMCI), the gradually changing patterns from HC to EMCI to LMCI to AD were also clearly observed (Fig. 5).

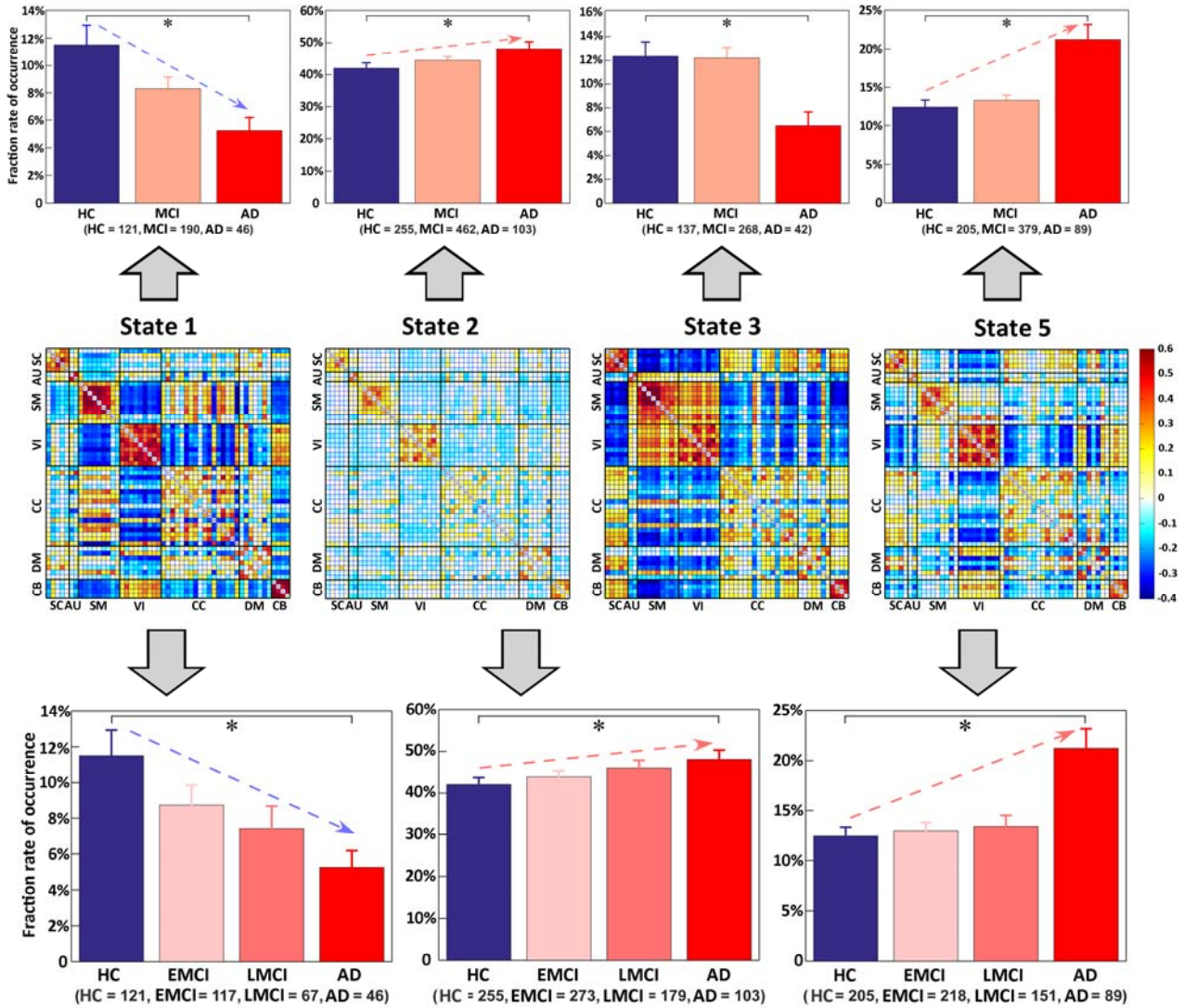

Fig. 5. The results of study 3. The results revealed gradually changing patterns from healthy controls (HCs) to early MCI (EMCI) to late MCI (LMCI) to Alzheimer's disease (AD), measured by dFNC measures. Upper: Group differences in the fraction rate of occurrences of dFNC states among HC, MCI, and AD. Middle: The discriminating dFNC states, along with the count of subjects that have at least one window clustered into the state. Bottom: Group differences in the fraction rate of occurrences of dFNC states among HC, EMCI, LMCI, and AD. Regarding the fraction rate of occurrences in each state, bar and error bar represent the mean and the standard error of mean, respectively. Significant group difference (false discovery rate corrected, $p = 0.05$) is indicated by asterisks.

Study 4: Bipolar disorder (BD) and major depressive disorder (MDD) can be successfully distinguished using brain spatial networks

In this study, we demonstrate that functional network measures derived using *NeuroMark* can be reliable features for differentiating patients with challenging disorders. We focused on classifying bipolar disorder (BD) and major depressive disorder (MDD), both of which can exhibit strong depressive symptoms and are difficult to distinguish in clinical diagnosis. The used features were ICNs computed using *NeuroMark* . Fig. 6 shows the pipeline and classification evaluation.

Based on an unbiased 10-fold cross-validation procedure on 32 BD and 34 MDD patients, the optimal ICN combination from different functional domains was selected and used to train support vector machine (SVM) classifiers within each training set, and then each subject in the testing set was classified. This resulted in a high mean of classification accuracy across 100 runs (overall accuracy: 91%, BD individual-class accuracy: 89%, MDD individual-class accuracy: 94%). If determining the final label of the testing data using a majority voting, the overall accuracy reached up 93.94% (BD individual-class accuracy 90.63%, MDD individual-class accuracy 97.06%). The discriminative ICNs with highest frequency (IC 56, IC 33, IC 40, IC 98, IC 80, and IC 20) involved the middle temporal gyrus, insula, precuneus, putamen, superior parietal, and inferior occipital gyrus.

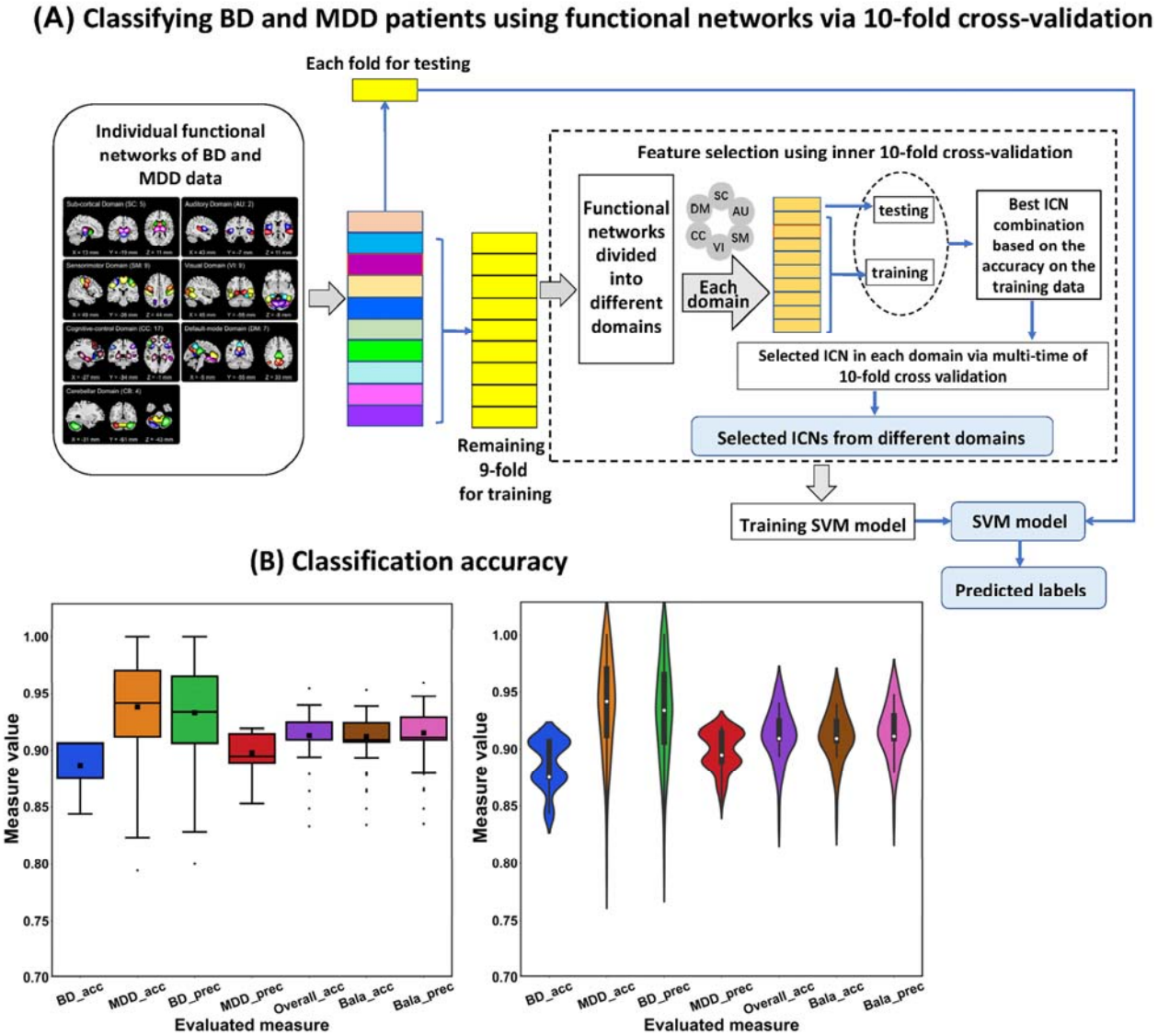

Fig. 6. The classification pipeline and accuracy in study 4. (A) The pipeline of classifying between BD and MDD patients using functional network maps as features, in which an unbiased 10-fold cross-validation procedure was applied. (B) The evaluated measures included individual-class accuracy (BD_acc and MDD_acc), individual-class precision (BD_Prec and MDD_prec), overall accuracy (Overall_acc), balanced accuracy (Bala_acc), and balanced precision (Bala_Prec). For each measure, we show the values from 100 runs using both boxplot and violinplot.

Discussion and Conclusion

Clinical diagnosis of the neuropsychiatric disorders overwhelmingly relies on the pattern of symptoms. Neuroimaging measures may hold more objective, biology-based quantification of brain abnormalities and consequently provide additional biomarkers to guide diagnosis and treatment. The complexity of the brain requires the neuroscience community to analyze big-data samples assembled from multi-site studies to achieve statistically powerful findings. Exploring clinically related brain disorders via large-scale analysis to understand their underlying mechanisms and relationship also

can help to redefine the disorder categories or develop new subtypes. Therefore, a standardized analysis framework is urgently needed to handle big data in the neuroscience field.

Characterizing inter-relationship of spatially distributed brain regions using fMRI has been important for providing biomarkers in the neuroscience filed. Numerous methods for delineating and estimating functional network/connectivity have been proposed to promote the progress of precision medicine on brain disorders. ICA holds the promising ability to extract network features that retain more individual-level variability. However, due to its data-driven nature, synthesis across ICA-derived results presents a challenge which can hinder replication and cross-study comparison.

In this paper, we proposed to use an Adaptive-ICA informed by reliable network priors to achieve linked analyses among different datasets, studies and disorders. We extended group network information [16] to independent replicated network templates for achieving individual variances while maintaining subject correspondence. In this paper, the network templates were obtained from two large-sample HC populations (1828 subjects) so as to minimize bias to a specific dataset to be analyzed. The use of such prior information can greatly reduce the search space and improve the likelihood of detecting useful markers [29].

To assess the efficacy of the proposed framework, we performed four studies employing a large sample of data (2454 subjects) relating to six brain disorders to evaluate the framework from different angles. Our results clearly support that the framework works well in finding reproducible network markers from different datasets, investigating relationship between disorders by linking multiple studies, exploring subtle differences between groups, as well as distinguishing disorders based on network features.

In study 1, the similar alterations in SZ were found between independent datasets by using network measures extracted from our framework. The primary common changes included the decreased positive connectivity between the sub-cortical regions and cerebellum as well as the diminished negative connectivity between the sub-cortical and auditory/sensorimotor regions. Our finding supports that sub-cortical regions such as thalamus and caudate are greatly affected in SZ. While sub-cortical regions have an important role in cognitive, affective, and social functions in humans [30], previous work also found functional abnormalities of these regions in SZ [31, 32]. The overall results indicate this framework to be a powerful tool for capturing reproducible biomarkers.

Study 2 shows that *NeuroMark* provides a way to link independent studies for pushing forward the understanding of brain disorders. By comparing the results from study 2 and 1, we found that SZ and ASD share common functional abnormalities in the sub-cortical, sensorimotor, auditory and cerebellar regions, among which the sub-cortical regions showed great overlapping impairments. Although SZ and ASD are currently conceptualized as distinct disorders, there are so much overlap such as social withdrawal and communication impairment [33]. Historically, schizophrenia and autism were once considered to be the same disorder expressed at different developmental periods. Our study provides evidence of their commonality from the view of brain function.

Study 3 validated that our framework can identify subtle difference between related disorders (taking MCI and AD for instance here). Compared to HCs, AD patients exhibited more occurrence in weakly connected states, consistent with the results found in other brain disorders, including bipolar disorder [34], schizophrenia [35, 36], and autism [37]. MCI showed similar trends as AD but with much weaker changes. These patterns position MCI as an intermediate stage between HC and AD. More interestingly, when we divided the MCI group into EMCI and LMCI, gradual changes were found in the dynamic features from HC to EMCI to LMCI to AD. The study showed that our framework can capture subtle dFNC differences that help to characterize the progression in cognitive impairment in dementia.

In Study 4, we used the spatial functional network features extracted via the *Neuromark* framework to distinguish complex brain disorders with similar symptoms. Using unbiased 10-fold cross-validation, we achieved a high classification accuracy (>90%) between BD and MDD patients that had overlapping depressive symptoms. The important discriminating brain regions involved the middle temporal gyrus, insula, precuneus, putamen, superior parietal and inferior occipital gyrus. Furthermore, the performance was better than a previous study [38], even though in the previous work the group-level ICs were computed based on the MDD and BD data themselves.

In general we found great promise of the *NeuroMark* framework, though there are still some limitations. One limitation of the framework is that the present network templates were obtained only based on two independent datasets. The templates can be progressively improved and refined as more data are included, hopefully to generate functional network templates with greater reproducibility. In addition, the current network templates were estimated under a high model-order (the number of ICs =100). In future we will explore network estimation under different parcellation

levels. Considering the ability to link different datasets, disorders and studies in our framework, we also plan to provide a cloud computation platform which implements this approach. Our hope is that by using this robust framework, functional network features can be widely studied and compared among numerous brain disorders.

A robust and generalized ICA framework was introduced in this paper for the analysis of fMRI datasets. In fact, the framework can be expanded to other modalities. Taking structural MRI for example, the source-based morphometry (SBM) [39, 40], a multivariate version of voxel-based morphometry (VBM), applies ICA to gray matter (GM) maps to detect common covariation among subjects and subject-associated weights. It is apparent that results of SBM vary across different datasets and runs. Using our method taking robust priors as guidance, the covariation patterns can be linked, thus resulting in comparable weights as features across different data (see regression based example here [41]). Group ICA is also useful for analyzing electroencephalography (EEG) data. Previous studies [42, 43] extracted EEG sources by concatenating the data across the spatial dimension (see also the EEGIFT software: http://trendscenter.org/software). Generating robust a priori sources to guide the individual source computation will be an ongoing effort.

In summary, we present a framework to generalize and standardize the calculation of possible brain imaging biomarkers which leverages the benefits of a data-driven approach to adapt to the individual data, while also providing comparability across multiple analyses. Results highlight the promise of the approach that we hope will be a useful stepping stone towards eventual application of such approaches in the clinic.

Methods

In the section, we first describe the proposed framework, and then introduce the methodology for the four example studies to assess the capacity of the proposed framework.

Approach for selecting data and computing brain mask

A rigorous criterion was implemented for subject selection to ensure high-quality data. For fMRI, we selected data with the properties: 1) data with head motions less than 3º rotations and 3 mm transitions along the whole scanning period; 2) data with more than 120 time points in fMRI acquisition; 3) data providing a successful normalization in the full brain. In terms of the third point,

whether fMRI data have good normalization to the template is important in group ICA. We evaluated the normalization quality of data by comparing the individual-subject mask and the group mask. This method was applied to each study's fMRI data separately. First, using the volume in the first time point, we calculated the individual mask for each subject by setting voxels showing greater values than 90% of the whole brain mean to 1. Next, we yielded a group mask by setting voxels included in more than 90% of the individual masks to 1. Then, for each subject, we calculated the correlations between the group mask and the individual mask. The correlations were calculated using voxels within the top 10 slices of the mask, within the bottom 10 slices of the mask, and within the whole mask, resulting in three correlation values for each subject. If a subject had correlations larger than the specified thresholds, we included this subject for further fMRI analysis. Finally, the group mask of each study was computed again based on the selected subjects' individual masks.

Identifying reliable functional network templates

The spatial network priors (i.e., the ICN templates) were obtained based on two independent HC datasets from the human connectome project (HCP, http://www.humanconnectomeproject.org/data/) and genomics superstruct project (GSP, https://www.nitrc.org/projects/gspdata). We preprocessed the GSP dataset using statistical parametric mapping (SPM12, http://www.fil.ion.ucl.ac.uk/spm/). Rigid body motion correction was performed to correct subject head motion, followed by the slice-timing correction to account for timing difference in slice acquisition. The fMRI data were subsequently warped into the standard Montreal Neurological Institute (MNI) space using an echo planar imaging (EPI) template and were slightly resampled to $3 \times 3 \times 3$ mm^3 isotropic voxels. The resampled fMRI images were further smoothed using a Gaussian kernel with a full width at half maximum (FWHM) = 6 mm. For the HCP dataset, we downloaded the preprocessed data from online and resliced them to the same spatial resolution ($3 \times 3 \times 3$ mm^3) with the preprocessed GSP data using SPM12. More details in terms of the preprocessing on HCP data can be found online (http://www.humanconnectomeproject.org/data/). After quality control, in total 1005 individuals the GSP dataset and 823 individuals from the HCP dataset were chosen (Table S1).

Table S1. The demographic information of the GSP and HCP data

	Subject number	Age: mean (std)	Gender: male (female)	Transitions: mean (std)	Rotations: mean (std)
GSP	1005	21.5373 (2.9629)	411 (594)	0.1416 (0.0920)	0.1426 (0.0962)
HCP	823	28.9721 (3.4250)	356 (467)	--	--

We conducted the following analysis for the GSP and HCP datasets, respectively, in order to obtain potential network templates. Regarding each individual, principle component analysis (PCA) was first performed to reduce fMRI data to 110 principal components (PCs), which preserved more than 95% variance of the original data. Then, the individual-level PCs of each subject were concatenated across different subjects (1005 subjects for GSP or 823 subjects for HCP) and reduced into 100 PCs via another PCA at the group level. Next, the Infomax algorithm [44] was used to decompose the 100 PCs into 100 ICs. This procedure was repeated 100 times using the ICASSO technique [45], in which the best ICA run was selected to generate 100 reliable group-level ICs for each dataset [46].

We matched the two groups of ICs using a greedy spatial correlation analysis to find replicated networks. Here, a spatial similarity matrix $\boldsymbol{C}$ (size: 100 × 100) was obtained by computing the absolute value of Pearson correlation coefficients between spatial maps of ICs from GSP and components from HCP. Based on the matrix $\boldsymbol{C}$, the pair of ICs with the maximum correlation value were selected and considered as the first-matched components pair. If their original correlation value was negative, one of the ICs was sign-flipped. After identifying a matched ICs pair, the correlation values related to them in the matrix $\boldsymbol{C}$ were set to zero, resulting in a new similarity matrix $\boldsymbol{C}_{\text{new}}$. As such, the matching procedure was repeated continually on updated correlation matrices, until the final matched IC pair was found. IC pairs are considered to be reproducible if they show a higher spatial correlation than a given threshold 0.4, a more strict threshold than previous work [47]. Next, we characterized a subset of these reproducible ICs as ICNs if they exhibited activation peaks in gray matter, had low spatial overlap with known vascular, ventricular, motion and other artifacts, and exhibited dominant low-frequency fluctuations in their TCs. Five fMRI experts carefully inspected those matched ICs, labeled meaningful ICNs and assigned them to different functional domains. ICs with more than three votes were identified as highly replicated ICNs. This resulted in two groups of highly similar ICNs from HCP and GSP dataset, respectively. Next, we selected the ICNs captured

from the GSP dataset as the spatial network templates as they exhibited lower noise than the ICNs from the other group. Hereinafter, we use N to denote the number of network templates. The high reproduction degrees between networks of the two datasets are shown in Fig. S1.

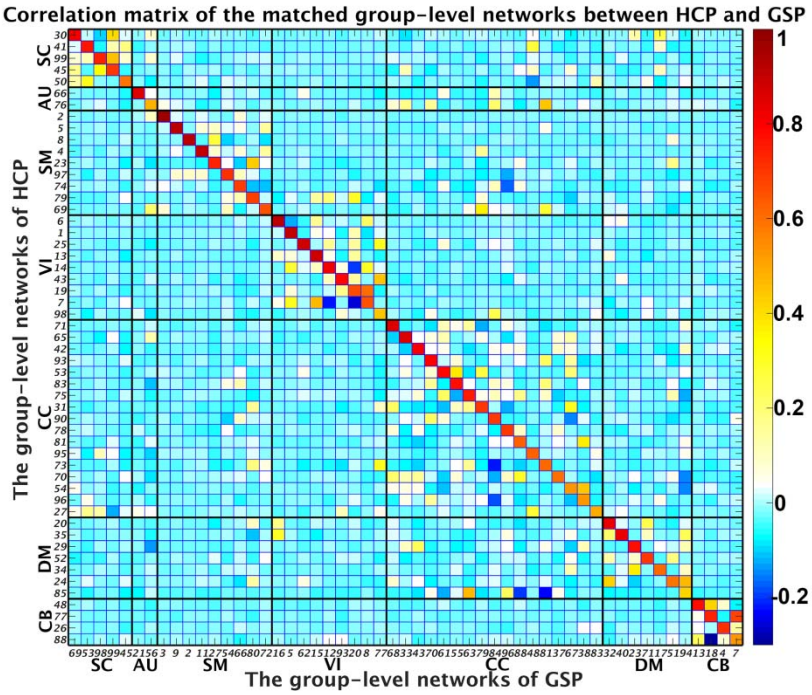

Fig. S1. The sorted spatial correlation matrix between the matched two groups of functional networks. It is seen that the diagonal values are high, indicating the selected network templates are common between the GSP and HCP data.

Estimating subject-specific functional brain networks

For each individual-subject fMRI data, ICNs are computed by Adaptive-ICA, an approach that adaptively estimates individual-level components using a prior define component templates. Two ICA algorithms [16, 26] available in the group ICA toolbox (GIFT) (http://trendscenter.org/software/) can be used for Adaptive-ICA. In this work, we applied the GIG-ICA [16] which uses a multiple-objective function optimization algorithm as shown in equation (1), by taking the obtained network templates and subject-specific fMRI data as input. Basically, there are two objective functions, one of which is to optimize the independence of networks in each subject's fMRI data, while the other is to optimize the comparability between one subject-specific network and its related network template. In the original GIG-ICA algorithm [12, 16], group-level components used as guidance are computed from its own group data. Here, we use the labeled and ordered network templates validated from two independent datasets as spatial priors to estimate individual networks. The

multiple-objective function represented in (1) was employed to compute one subject-specific network using a network template as guidance.

$$max \begin{cases} J(S_l^k) = \{E[G(S_l^k)] - E[G(v)]\}^2 \\ F(S_l^k) = E[S_l S_l^k] \end{cases}, \quad (1)$$

$$s.t. \quad \|w_l^k\| = 1.$$

In (1), S_l denotes the lth network template, and $S_l^k = (w_l^k)^T \cdot \widetilde{X^k}$ represents the estimated corresponding network of the kth subject, where $\widetilde{X^k}$ is the whitened X^k representing fMRI data matrix of the kth subject. Here, w_l^k is the unmixing column vector, which is to be solved in the optimization functions. The first function is for optimizing the independence measure of S_l^k, which is reflected using $J(S_l^k)$, i.e., the negentropy of S_l^k. Here, v is a Gaussian variable with zero mean and unit variance; $G(\cdot)$ is a nonquadratic function. The second function $F(S_l^k)$ is used to measure the comparability between S_l and S_l^k. $E[\,]$ denotes the expectation of variable. To solve the multiple-objective function optimization, a linear weighted sum method is applied to combine the two objective functions [16]. After the optimization, one subject-specific network can be obtained. Finally, for each subject, all N subject-specific networks corresponding to the N network templates and their relevant TCs are estimated from the data. Therefore, using this framework, all individual networks and their related TCs will not only be comparable across different datasets/studies/disorders as well as between previously analyzed data and new coming impendent data, but also show subject-unique characteristics in brain functional networks and their fluctuations.

Functional brain network features

Using the proposed framework, multiple network features (in addition to the original ICNs and TCs) can be computed, including the interactions between ICNs, graph measures of functional organization, frequency information of networks' fluctuations, as well as dynamic measures on both ICNs and their interactions. Taking network interaction as an example, static FNC (sFNC) can be obtained by computing the correlations between post-processed TCs of ICNs to yield sFNC matrix. Specifically, the steps to remove remaining noise sources of TCs include 1) detrending linear, quadratic, and cubic trends; 2) conducting multiple regressions of the 6 realignment parameters and their temporal derivatives; 3) de-spiking detected outliers; and 4) band-pass filtering with [0.01-0.15]

Hz. Thus, each element of sFNC matrix represents the connectivity between a pair of functional networks. While the ICN reflects intra-connectivity within network, the FNC matrix represents inter-connectivity strengths between different ICNs. The dynamic FNC (dFNC) also can be investigated through a sliding window approach. A tapered window, obtained by convolving a rectangle with a Gaussian, is often used to segment the entire TC of each ICN into several short TCs. For each window, the covariance matrix is then computed using the windowed TCs from different networks to measure the functional connectivity between ICNs within the window. To assess more accurate covariance matrix, a graphical LASSO method is usually applied to estimate the regularized inverse covariance matrix and then the covariance matrix from the inverse covariance matrix. For each subject, the covariance matrix of each window can be concatenated to form an array (size: $N \times N \times T$, here N is the number of ICNs and T is the number of windows), representing the dynamic changes of FNC along different windows.

Studies for evaluating the framework

Study 1: Investigating static functional network connectivity (sFNC) changes in schizophrenia (SZ): a replication study

In the first study, we assessed the ability of *NeuroMark* to identify reproducible biomarkers between different datasets. The proposed framework was implemented on two independent datasets, in order to detect brain changes of SZ patients relative to healthy controls. One dataset was from the Function Biomedical Informatics Research Network (FBIRN) including 210 SZ patients and 195 HCs. The other dataset were collected at the University of Maryland, Maryland Psychiatric Research Center (MPRC), including 251 SZ patients and 327 HCs. Resting-state fMRI data of SZ patients and HCs was preprocessed using the same preprocessing pipeline as for the GSP dataset and same criteria were used for subject selection. We retained 137 SZ patients and 144 HCs in the FBIRN dataset, and 150 SZ patients and 238 HCs in the MPRC dataset for the further analysis.

Using the N ICN templates as priors, we performed Adaptive-ICA on each individual-subject fMRI dataset to extract spatial subject-level ICNs and their related TCs. Next, a sFNC matrix was obtained for each subject via computing Pearson correlation coefficients between the post-processed TCs. We averaged the individual sFNC matrices across subjects for the FBIRN and MPRC data, separately, to validate if the connectivity patterns were comparable. Next, for each connection between two ICNs in the sFNC matrix, we investigated difference between HCs and SZ patients by

performing a two-tailed two-sample t-test ($p < 0.05$ with Bonferroni correction) for the FBIRN and MPRC datasets, separately, after regressing out age, gender and site effects. Finally, we investigated if the identified changes in SZ are reproducible between the two datasets by comparing their two-sample t-test results.

Study 2: Investigating the common static functional network connectivity (sFNC) alterations in autism spectrum disorder (ASD) and SZ: multi-study comparison

Since we computed the brain functional network templates using data from large-sample healthy population independent from the data being analyzed, it is feasible to link multiple independent studies. In study 2, we explored sFNC changes in ASD compared to HCs and then evaluated the common impairments between SZ and ASD by summarizing the results from this analysis and study 1, each of that was performed independently of the other. We selected data from Autism Brain Imaging Data Exchange I (ABIDEI), provided by the National Institute of Mental Health. The ABIDEI dataset involves 17 sites and includes a total of 539 individuals with ASD and 573 age-matched HCs. We conducted preprocessing and subject selection using the same pipeline and criterion. After quality control, 398 ASD individuals and 471 HCs in the ABIDEI dataset remained.

Based on the *Neuromark* framework, we obtained N individual ICNs and then estimated their functional interaction (i.e. sFNC) for each subject. Furthermore, we investigated the HC vs. ASD differences on sFNC measures using two-tailed two-sample t-tests ($p < 0.05$ with Bonferroni correction). Since the features were extracted using a same way, it was possible to compare the symptom-related disorders (i.e. SZ and ASD) in terms of their overlapping alterations relative to HCs based on the results from study 1 and 2. We then evaluated the commonality between SZ and ASD in sFNC impairments relative to HCs.

Study 3: Evaluating levels of cognitive performance/impairment linked to dynamic FNC

In this study, we investigated dynamic brain changes among Alzheimer's disease (AD) patients, mild cognitive impairment (MCI) patients, and HCs. We used the publicly available Alzheimer's Disease Neuroimaging Initiative (ADNI) dataset, which collected resting-state fMRI data from 275 HCs, 107 Alzheimer's Disease (AD) patients and 480 Mild Cognitive Impairment (MCI) patients. Using the same preprocessing and subject selection procedures, we had a total of 838 subjects (104 patients with AD, 470 patients with MCI, and 264 HCs) for analysis.

For each subject, we estimated dFNC using a sliding window approach [17]. Since the datasets have different temporal resolutions, we performed interpolation on the TCs with longer TR to construct new TCs with the same nominal temporal resolution as those data with smallest TR and the same length of data. This procedure helps to control the potential impacts on the dynamic analysis caused by the different temporal resolutions. The tapered window was obtained by convolving a rectangle (window size = 40 TRs = 24.3 s) with a Gaussian ($\sigma = 3$) function. This window was slid in steps of 1 TR, resulting in total $T = 468$ windows for yielding dFNC matrices.

A K-means clustering analysis [17] was implemented on dFNC estimates to capture occurred states in time and across subjects. L1 norm was used as the distance function with the upper triangular ($N \times (N-1)/2$) values in the matrices as features. The optimal number of clusters was determined as 5 by the elbow criterion, which was within a reasonable range (4~7) consistent with the previous dFNC studies on different brain disorders [34, 37, 48-50].

Regarding each state, we computed its fraction rate of occurrence for each subject by computing the percentage of the number of time windows assigned to the state in the number of total windows. To investigate group differences in the fraction rate of each state, ANOVA was performed after regressing out age and gender. If the ANOVA resulted in a significant diagnosis effects, a generalized linear model (GLM) including age and gender was conducted to examine the group difference between any paired groups.

Study 4: Classification of two disorders with overlapping symptoms using spatial networks

In this study, we aimed to employ network features identified by the proposed framework for the classification of symptom-related disorders. Resting-state fMRI data from 32 patients with BD Type I and 34 patients with MDD were included. More details can be found in a previous study [38]. We conducted the preprocessing and subject selection using the same pipeline and criterion as other studies. Based on spatial network (i.e. ICN) features, we assessed the ability to distinguish the MDD and BD patients.

Using *NeuroMark*, the individual ICNs were estimated by taking the selected network templates as guidance after discarding cerebellum-related templates, due to cerebellum being partially missing in the scanned data. In order to evaluate if the ICNs can be powerful features to classify BD and MDD patients, we applied an unbiased 10-fold cross-validation framework, in which nine of ten folds were used as the training data and the remaining fold was used as the testing data successively.

Consistent to the previous work [38], we applied support vector machine with sigmoid kernel for classification. The feature selection and model training were performed only based on the training data.

Feature selection plays a key role in classification, especially for the high-dimensional network measures. In this work, we extracted the most discriminative ICN from each functional domain, and then combined the discriminative ICNs from all functional domains as features. In order to find the most discriminative ICN for each domain, we used an inner 10 times of 10-fold cross-validation procedure within the training set based on a forward ICN-selection technique. Basically, the ICNs were added one by one based on the classification accuracy on the inner testing data, evaluated using the model built using the inner training data. Then, for each run in the inner 10-fold procedure, the optimal ICN combination corresponding to the highest classification accuracy can be found. The ICN with the highest occurring frequency in the optimal ICN combination sets (across different repeats) was validated as the most-discriminative ICN for that domain. After that, the combined discriminative ICNs from different domains were used as features to train the outer training data. While the previous study [38] that used group information from its own data, individual-level ICN features computed using our framework were more unbiased.

To quantify the classification results, we evaluated multiple measures including the individual class accuracy, individual class precision, overall accuracy, balanced accuracy and balanced precision [51] based on the predicted and diagnosis labels. Different measures reflect the results from different angles. The individual class accuracy reported the ratio of correctly classified subjects of a particular class to the total number of subjects in the class. The individual class precision was defined as the number of correctly classified subjects of a particular class divided by the total number of subjects predicted as the class. The overall accuracy was computed as the ratio of correctly classified subjects of all classes to the total number of subjects of all classes. Additionally, we also computed the mean of individual class accuracies, called as the balanced accuracy. The individual class precision values were also averaged to represent the balanced precision. For each measure, we show the results from different repeats using both boxplot and violinplot.

Data availability

The data that support the findings of this study are available from the corresponding author, upon reasonable request.

Acknowledgement

This work was supported by National Natural Science Foundation of China (Grant No. 61703253 to YHD, 61773380 to JS), National Institutes of Health grants 5P20RR021938/P20GM103472 & R01EB020407 and National Science Foundation grant 1539067 (to VDC).

Data collection and sharing for Study 3 was funded by the Alzheimer's Disease Neuroimaging Initiative (ADNI) (National Institutes of Health Grant U01 AG024904) and DOD ADNI (Department of Defense award number W81XWH-12-2-0012). ADNI is funded by the National Institute on Aging, the National Institute of Biomedical Imaging and Bioengineering, and through generous contributions from the following: AbbVie, Alzheimer's Association; Alzheimer's Drug Discovery Foundation; Araclon Biotech; BioClinica, Inc.; Biogen; Bristol-Myers Squibb Company; CereSpir, Inc.; Cogstate; Eisai Inc.; Elan Pharmaceuticals, Inc.; Eli Lilly and Company; EuroImmun; F. Hoffmann-La Roche Ltd and its affiliated company Genentech, Inc.; Fujirebio; GE Healthcare; IXICO Ltd.; Janssen Alzheimer Immunotherapy Research & Development, LLC.; Johnson & Johnson Pharmaceutical Research & Development LLC.; Lumosity; Lundbeck; Merck & Co., Inc.; Meso Scale Diagnostics, LLC.; NeuroRx Research; Neurotrack Technologies; Novartis Pharmaceuticals Corporation; Pfizer Inc.; Piramal Imaging; Servier; Takeda Pharmaceutical Company; and Transition Therapeutics. The Canadian Institutes of Health Research is providing funds to support ADNI clinical sites in Canada. Private sector contributions are facilitated by the Foundation for the National Institutes of Health (www.fnih.org). The grantee organization is the Northern California Institute for Research and Education, and the study is coordinated by the Alzheimer's Therapeutic Research Institute at the University of Southern California. ADNI data are disseminated by the Laboratory for Neuro Imaging at the University of Southern California.

References:

1. Woo, C.W., Chang, L.J., Lindquist, M.A. & Wager, T.D. Building better biomarkers: brain models in translational neuroimaging. *Nature neuroscience* **20**, 365-377 (2017).

2. Poline, J.B., *et al.* Data sharing in neuroimaging research. *Front Neuroinform* **6**, 9 (2012).

3. Poldrack, R.A. & Gorgolewski, K.J. Making big data open: data sharing in neuroimaging. *Nature neuroscience* **17**, 1510-1517 (2014).

4. Dosenbach, N.U., *et al.* Prediction of individual brain maturity using fMRI. *Science* **329**, 1358-1361 (2010).

5. Tzourio-Mazoyer, N., *et al.* Automated anatomical labeling of activations in SPM using a macroscopic anatomical parcellation of the MNI MRI single-subject brain. *Neuroimage* **15**, 273-289 (2002).

6. Zang, Y., Jiang, T., Lu, Y., He, Y. & Tian, L. Regional homogeneity approach to fMRI data analysis. *Neuroimage* **22**, 394-400 (2004).

7. McKeown, M.J., Hansen, L.K. & Sejnowsk, T.J. Independent component analysis of functional MRI: what is signal and what is noise? *Curr Opin Neurobiol* **13**, 620-629 (2003).

8. Calhoun, V.D. & Adali, T. Multisubject independent component analysis of fMRI: a decade of intrinsic networks, default mode, and neurodiagnostic discovery. *IEEE reviews in biomedical engineering* **5**, 60-73 (2012).

9. Calhoun, V.D., Adali, T., Pearlson, G.D. & Pekar, J.J. A method for making group inferences from functional MRI data using independent component analysis. *Human brain mapping* **14**, 140-151 (2001).

10. Du, Y.H., Li, H.M., Wu, H. & Fan, Y. Identification of subject specific and functional consistent ROIs using semi-supervised learning. *Proceedings of SPIE, Medical Imaging 2012: Image Processing* **8314** (2012).

11. Yu, Q.B., *et al.* Comparing brain graphs in which nodes are regions of interest or independent components: A simulation study. *Journal of neuroscience methods* **291**, 61-68 (2017).

12. Du, Y.H., *et al.* Artifact removal in the context of group ICA: A comparison of single-subject and group approaches. *Human brain mapping* **37**, 1005-1025 (2016).

13. Xu, J., *et al.* Functional network overlap as revealed by fMRI using sICA and its potential relationships with functional heterogeneity, balanced excitation and inhibition, and sparseness of neuron activity. *PloS one* **10**, e0117029 (2015).

14. Calhoun, V.D. & de Lacy, N. Ten Key Observations on the Analysis of Resting-state Functional MR Imaging Data Using Independent Component Analysis. *Neuroimaging clinics of North America* **27**, 561-579 (2017).

15. Beckmann, C., Mackay, C., Filippini, N. & Smith, S. Group comparison of resting-state FMRI data using multi-subject ICA and dual regression. *NeuroImage* **47 Supplement 1**, S148 (2009).

16. Du, Y.H. & Fan, Y. Group information guided ICA for fMRI data analysis. *NeuroImage* **69**, 157-197 (2013).

17. Allen, E.A., *et al.* Tracking whole-brain connectivity dynamics in the resting state. *Cerebral cortex* **24**, 663-676 (2014).

18. Marusak, H.A., *et al.* Dynamic functional connectivity of neurocognitive networks in children. *Human Brain Mapping* **38**, 97-108 (2017).

19. Rashid, B., *et al.* Classification of schizophrenia and bipolar patients using static and dynamic resting-state fMRI brain connectivity. *NeuroImage* **134**, 645-657 (2016).

20. Demirci, O., Clark, V.P. & Calhoun, V.D. A projection pursuit algorithm to classify individuals using fMRI data: Application to schizophrenia. *NeuroImage* **39**, 1774-1782 (2008).

21. Colibazzi, T. Journal Watch review of Research domain criteria (RDoC): Toward a new classification framework for research on mental disorders. *Journal of the American Psychoanalytic Association* **62**, 709-710 (2014).

22. Cosgrove, V.E. & Suppes, T. Informing DSM-5: biological boundaries between bipolar I disorder, schizoaffective disorder, and schizophrenia. *Bmc Med* **11**, 127 (2013).

23. Hommer, R.E. & Swedo, S.E. Schizophrenia and autism-related disorders. *Schizophr Bull* **41**, 313-314 (2015).

24. Zuo, X.N., *et al.* An open science resource for establishing reliability and reproducibility in functional connectomics. *Scientific data* **1**, 140049 (2014).

25. Noble, S., Scheinost, D. & Constable, R.T. A decade of test-retest reliability of functional connectivity: A systematic review and meta-analysis. *NeuroImage*, 116157 (2019).

26. Lin, Q.H., Liu, J., Zheng, Y.R., Liang, H. & Calhoun, V.D. Semiblind spatial ICA of fMRI using spatial constraints. *Human brain mapping* **31**, 1076-1088 (2010).

27. Du, Y.H., *et al.* Comparison of IVA and GIG-ICA in Brain Functional Network Estimation Using fMRI Data. *Frontiers in neuroscience* **11: 267** (2017).

28. Salman, M.S., *et al.* Group ICA for Identifying Biomarkers in Schizophrenia: 'Adaptive' Networks via Spatially Constrained ICA Show More Sensitivity to Group Differences than Spatio-temporal Regression. *NeuroImage. Clinical* **22**, 101747 (2019).

29. Cohen, J.D., *et al.* Computational approaches to fMRI analysis. *Nature neuroscience* **20**, 304-313 (2017).

30. Koshiyama, D., *et al.* Role of subcortical structures on cognitive and social function in schizophrenia. *Sci Rep* **8**, 1183 (2018).

31. Woodward, N.D., Karbasforoushan, H. & Heckers, S. Thalamocortical dysconnectivity in schizophrenia. *The American journal of psychiatry* **169**, 1092-1099 (2012).

32. Kirino, E., *et al.* Functional Connectivity of the Caudate in Schizophrenia Evaluated with Simultaneous Resting-State Functional MRI and Electroencephalography Recordings. *Neuropsychobiology* **77**, 165-175 (2019).

33. Ford, T.C., Apputhurai, P., Meyer, D. & Crewther, D.P. Confirmatory factor analysis of autism and schizophrenia spectrum traits. *Pers Indiv Differ* **110**, 80-84 (2017).

34. Rashid, B., Damaraju, E., Pearlson, G.D. & Calhoun, V.D. Dynamic connectivity states estimated from resting fMRI Identify differences among Schizophrenia, bipolar disorder, and healthy control subjects. *Frontiers in human neuroscience* **8**, 897 (2014).

35. Damaraju, E., *et al.* Dynamic functional connectivity analysis reveals transient states of dysconnectivity in schizophrenia. *NeuroImage: Clinical* **5**, 298-308 (2014).

36. Du, Y.H., *et al.* Interaction among subsystems within default mode network diminished in schizophrenia patients: A dynamic connectivity approach. *Schizophrenia research* **170**, 55-65 (2016).

37. Fu, Z., *et al.* Transient increased thalamic-sensory connectivity and decreased whole-brain dynamism in autism. *NeuroImage* (2018).

38. Osuch, E., *et al.* Complexity in mood disorder diagnosis: fMRI connectivity networks predicted medication-class of response in complex patients. *Acta Psychiatr Scand* **138**, 472-482 (2018).

39. Xu, L., Groth, K.M., Pearlson, G., Schretlen, D.J. & Calhoun, V.D. Source-Based Morphometry: The Use of Independent Component Analysis to Identify Gray Matter Differences With Application to Schizophrenia. *Human brain mapping* **30**, 711-724 (2009).

40. Bergsland, N., *et al.* Gray matter atrophy patterns in multiple sclerosis: A 10-year source-based morphometry study. *NeuroImage. Clinical* **17**, 444-451 (2018).

41. Silva, R.F., *et al.* The tenth annual MLSP competition: Schizophrenia classification challenge. *2014 IEEE International Workshop on Machine Learning for Signal Processing (MLSP)*, 1-6 (2014).

42. Huster, R.J., Plis, S.M. & Calhoun, V.D. Group-level component analyses of EEG: validation and evaluation. *Frontiers in neuroscience* **9**, 254 (2015).

43. Huster, R.J. & Raud, L. A Tutorial Review on Multi-subject Decomposition of EEG. *Brain Topogr* **31**, 3-16 (2018).

44. Bell, A.J. & Sejnowski, T.J. An information-maximization approach to blind separation and blind deconvolution. *Neural computation* **7**, 1129-1159 (1995).

45. Himberg, J. & Hyvarinen, A. ICASSO: Software for investigating the reliability of ICA estimates by clustering and visualization. *2003 Ieee Xiii Workshop on Neural Networks for Signal Processing - Nnsp'03*, 259-268 (2003).

46. Ma, S., *et al.* Automatic identification of functional clusters in FMRI data using spatial dependence. *IEEE transactions on bio-medical engineering* **58**, 3406-3417 (2011).

47. Smith, S.M., *et al.* Correspondence of the brain's functional architecture during activation and rest. *Proc Natl Acad Sci U S A* **106**, 13040-13045 (2009).

48. Fu, Z., *et al.* Altered static and dynamic functional network connectivity in Alzheimer's disease and subcortical ischemic vascular disease: shared and specific brain connectivity abnormalities. *Human Brain Mapping* (2019).

49. Du, Y., *et al.* Dynamic functional connectivity impairments in early schizophrenia and clinical high-risk for psychosis. *NeuroImage* **180**, 632-645 (2018).

50. Abrol, A., *et al.* Replicability of time-varying connectivity patterns in large resting state fMRI samples. *NeuroImage* **163**, 160-176 (2017).

51. Cuadros-Rodriguez, L., Perez-Castano, E. & Ruiz-Samblas, C. Quality performance metrics in multivariate classification methods for qualitative analysis. *Trac-Trend Anal Chem* **80**, 612-624 (2016).